Improving temporal resolution and speed sensitivity of laser speckle contrast analysis imaging based on noise reduction with an anisotropic diffusion filter

Lipei Song[1,3], Xueyan Wang[2], Ru Zhang[1] ⓘ, Kuanshou Zhang[3], Zhen Zhou[2,5] and Daniel S Elson[4,5]

[1] Institute of Modern Optics, Nankai University, Tianjin, 300350, People's Republic of China
[2] Department of Acupuncture Cerebropathy, Second Affiliated Hospital of Tianjin University of TCM, Tianjin, 300150, People's Republic of China
[3] State Key Laboratory of Quantum Optics and Quantum Optics Devices, Institute of Opto-Electronics, Shanxi University, Taiyuan 030006, People's Republic of China
[4] Department of Surgery and Cancer, Imperial College London, London, SW7 2AZ, United Kingdom

E-mail: zhouzhen7681@126.com and daniel.elson@imperial.ac.uk

CrossMark

Abstract

The fluctuation of contrast caused by statistical noise degenerates the temporal/spatial resolution of laser speckle contrast imaging (LSCI) and limits the maximum speed when imaging. In this study, we investigated the application of the anisotropic diffusion filter (ADF) to temporal LSCI and found that the edge magnitude parameter of the ADF can be determined by the mean of the contrast image. Because the edge magnitude parameter is usually denoted as K, we term this the K-constant ADF (KC-ADF) and show that temporal sensitivity is improved when imaging because of the enhanced signal-to-noise ratio when using the KC-ADF in small-animal experiments. The cardiac cycle of a rat as high as 390 bpm can be imaged with an industrial camera.

Keywords: laser speckle contrast imaging, temporal resolution, anisotropic diffusion filter, signal-to-noise ratio, speed sensitivity

(Some figures may appear in colour only in the online journal)

1. Introduction

Laser speckle contrast imaging (LSCI) allows the movement of scatters—and hence blood flow—to be imaged via the spatial and temporal variations in interference that result. Ideally, LSCI contrast values should be identical in areas with the same particle velocity distribution, but in reality there are fluctuations caused by statistical residuals that result in speckle contrast noise. Duncan *et al* investigated the statistical properties of local contrast and found that it follows a log-normal distribution [1]. This contrast noise degrades the appearance of *in vivo* contrast images, especially when the blood vessels are small and the change of blood flow speed is small; sometimes the contrast changes introduced by the flow speed in the vessel area can be obscured by the contrast noise.

Different methods have been investigated to increase the signal-to-noise ratio (SNR) and spatial or temporal resolution. Averaging temporal contrast over a spatial window (t_{avg}sLSCI) [2] and averaging spatial contrast values over a temporal window (s_{avg}tLSCI) [3], calculating the contrast while taking both temporal and spatial changes into consideration (stLSCI) [4], and simply increasing the number of frames for the calculation have been investigated. Miao *et al*

---

[5] Authors to whom any correspondence should be addressed.

utilized the concept of histogram equalization over a sequence of contrast images to enhance the contrast image [5]. They later proposed a method using a random process estimator to improve the SNR and spatiotemporal resolution [6]. Qiu *et al* [7] compensated for the contrast bias introduced by the speckle size to improve the SNR and spatial resolution, which is also demonstrated in reference [8]. In the frequency domain, Zeng *et al* calculated the intensity fluctuation modulation instead of the contrast and recovered higher spatial resolution than that in conventional contrast images [9]. These methods either depend on larger data-sets or compromise spatial–temporal resolution to achieve the desired results.

To preserve the structure of vessels, Rege *et al* introduced anisotropic processing to calculate the contrast along the blood flow direction [10] and Li *et al* combined segmentation [11], a rigid-tracking algorithm [12] and speckle-reducing anisotropic diffusion (SRAD) [13] to improve spatial–temporal resolution.

Anisotropic diffusion filtering (ADF) is a common method for removing speckles in ultrasonic imaging [13–15]. Compared to other common spatial filters such as the Gaussian filter, it is an edge-sensitive averaging filter. The smoothing is perpendicular to the detected edges, therefore preserving the spatial structures while removing noise. So it is ideal for the smoothing of LSCI images and for preserving vessel structure. In contrast with SRAD, it is able to remove additive noise and is easier to apply. Further improvements in basic Perona–Malik ADF [16] have been proposed such as robust ADF [17] and median-boosted anisotropic diffusion techniques [18], to determine the filter parameters more accurately and robustly and to optimize the performance of the filter. In these methods the edge magnitude parameter (K) is the key to the design of the filter and its output. It is usually manually chosen, set by a noise estimator such as a canny noise estimator or determined from Pratt's figure of merit [19].

In this paper, we investigate the application of ADF to LSCI images and demonstrate that the K value can be simply determined by the mean of the contrast image based on the cumulative density function (CDF) of the gradients of the contrast image. We also demonstrate that a K value between 0.17 and 0.254 for the processed contrast image results in no obvious image degradation. This suggests the possibility of using a constant K value for all contrast images. We call this ADF the K-constant anisotropic diffusion filter (KC-ADF). In addition, we require three speckle frames for a single temporal contrast image calculation and two of the three frames may be reused for the next adjacent contrast image calculation. We imaged the contrast changes during a rat cardiac cycle, demonstrating an improvement of the speed sensitivity and temporal resolution. This method will prove to be a useful tool for imaging high-velocity changes and will benefit the detection, diagnosis, characterization and treatment of blood circulatory diseases particularly in animal models.

2. Methods

2.1. Filter design

The ADF used in this paper is based on the Perona–Malik diffusion kernel with four neighborhoods [16, 17]:

$$C(i, j, n + 1) = C(i, j, n) + \lambda(d_{\mathrm{N}} \cdot \nabla C_{\mathrm{N}} + d_{\mathrm{S}} \cdot \nabla C_{\mathrm{S}} + d_{\mathrm{E}} \cdot \nabla C_{\mathrm{E}} + d_{\mathrm{W}} \cdot \nabla C_{\mathrm{W}}).$$

(1)

It is an iterative process where $C(i, j, n)$ is the contrast value at pixel (i, j) in the nth iteration, which has the raw speckle contrast image as the initial input; λ is the rate of diffusion and is taken as 0.25 because we use four neighborhoods (pixels in the north, south, east and west directions); ∇C stands for the contrast gradients that are calculated from the value difference between adjacent pixels in specific directions; d denotes the diffusion coefficients; and the subscripts N, S, E, and W denote the directions north, south, east and west. The value of d in each direction can be calculated from the contrast gradient in that direction according to the following equation:

$$d = \frac{1}{1 + \left(\frac{|\nabla C|}{K}\right)^2}$$

(2)

where K is the edge magnitude parameter, the gradient threshold that determines whether the value will be increased or decreased during processing. As is mentioned above, a canny noise estimator finds the proper threshold K for a whole image; we borrowed the concept wherein the values taking up 90% of the CDF are valid and others are noise [19, 20] to investigate the value of K for differently blurred speckle images. For this purpose, a simulation was first implemented using speckle images synthesized with the method described in [20]. From the simulation, the relationship between the proper K value from the CDF and the mean of the contrast image was fitted and the result was then used for the *in vivo* experiment (see next sections). The CDF was calculated from the gradient of the contrast. The whole-image processing was implemented with Matlab.

2.2. Temporal-resolution-improved contrast image calculation

Contrast was calculated based on a statistical analysis, so the higher the number of samples used, the closer the result was to the estimate. Including more frames in tLSCI decreases the temporal resolution of the system; in contrast, including fewer frames increases the deviation of the contrast estimate and introduces a higher noise level. Therefore, we attempt to increase the temporal resolution by minimizing the time between two adjacent contrast images and decrease the deviation with the ADF.

Three frames are the minimum number of frames that can be used to calculate tLSCI. Therefore to improve the temporal resolution of tLSCI, three raw speckle images were included for calculating a single contrast image, and the two latter speckle images were subsequently reused in the calculation of
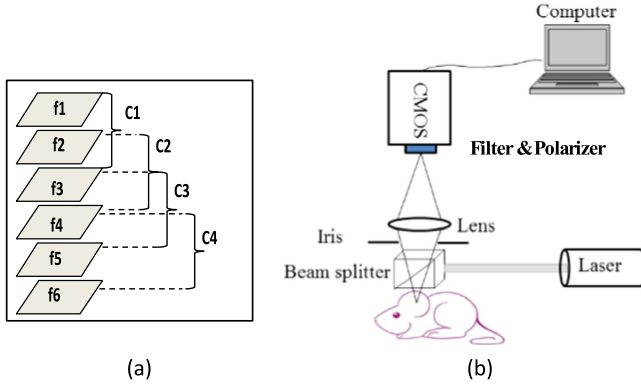
Figure 1. (a) Representation of raw stLSCI contrast image generation. (b) The experiment setup for imaging a rat ear.

the next adjacent contrast image [10]. In this way, the temporal resolution can be improved to be equal to the frame rate of the camera. The flow chart of the raw contrast calculation is shown in figure 1(a), where the speckle images are labeled f*n*, the raw contrast images are labeled C*n*, and the subscripts '1, 2, 3…' denote the frame index. For example, C1 is calculated from the first three speckle frames f1, f2 and f3; C2 is calculated from f2, f3, and f4, etc.

Therefore the calculation of the contrast can be expressed as:

$$C_{(x,y),i} = \frac{\frac{1}{2}\sqrt{\sum_{m=i}^{i+2}(I_{(x,y),m} - \mu_{(x,y),i})^2}}{\mu_{(x,y),i}} \qquad (3)$$

where $C_{(x,y),i}$ is the contrast value at pixel (x, y) in the *i*th contrast image, $i = 1, 2, 3 \cdots$; $\mu_{(x,y),i}$ is the mean intensity value of three successive speckle frames at pixel (x, y) and is calculated from:

$$\mu_{(x,y),i} = \frac{\sum_{m=i}^{i+2} I_{(x,y),m}}{3}; \qquad (4)$$

and $I_{(x,y),m}$ is the intensity of pixel (x, y) in the *m*th speckle image.

3. Simulation

In this section, the speckle image generation used the simulation method described in [21] and the speckle size was equal to 3 pixels [22].

An initial simulation examined the relationship between the mean contrast and the value of K, i.e. the contrast gradient value when the CDF of the gradient of the contrast was equal to 0.9. It can be understood that the faster the flow speed, the more blurred the speckle image and therefore the lower the contrast and contrast gradient. We synthesized 20 stacks of speckle images, where each stack contained three speckle frames, between which the correlation coefficients were identical and predefined. The correlation coefficients used for the 20 stacks were 0.05 to 1 with an increment of 0.05. Then the temporal contrast of every stack was calculated followed by the calculation of the CDF of the contrast gradient and the

mean of every contrast image. The value of K was extracted and the function between these K values and the mean contrast was analyzed.

In a second simulation, an initial spatial correlation map was defined and three fully developed speckle images were synthesized. The correlation distribution between these three speckle images and the reference speckle image was the initial correlation map multiplied by three correlation coefficients 0.95, 0.75 and 0.55 respectively for the defined regions of the image. As a result, we simulated a temporal sequence of three speckle images with a predefined spatial and temporal correlation distribution. The temporal contrast was calculated from these three speckle images. The three correlation coefficient values were specifically chosen to generate a contrast image with clear variations in spatial contrast. Then ADFs with different K values were applied to the contrast images to evaluate the noise deduction effect of the ADFs in the image domain.

4. *In vivo* experiment

A Sprague Dawley rat was anesthetized by injecting 10% chloral hydrate solution (0.3 ml / 100 g) prior to the experiment. An electrocardiogram (ECG) of the heartbeat was acquired and recorded with the Matlab system (Manjing Medease Science and Technology Co., Ltd) to compare with the results from the laser speckle contrast calculation. The experiment was conducted under approved guidelines and was reviewed by the institutional animal use committee of the Second Affiliated Hospital of Tianjin University of TCM. The ear of the rat was fixed on a solid block and was parallel with the optical table to isolate undesired movement.

The setup is shown in figure 1(b). The laser beam (671 nm, Changchun Laser Optoelectronics Technology Co., Ltd, China) was expanded to a diameter of 10 mm and illuminated the ear of the rat via a beam splitter. The rat ear was imaged by an achromatic lens ($f = 50$ mm, China Daheng Group, Inc.) and captured by a CMOS camera (1040 × 1280, Flea 3 USB 3.0, Point Grey, Canada). The filter and the polarizer in front of the camera removed environmental light and preferentially passed light of the same polarization state as the illumination. Because rat cardiac frequency is usually higher than 300 bpm, the camera was run in a binning mode of 2 × 2 pixels to achieve its maximum frame rate of 81 fps at an exposure time of 1 ms. The exposure time was set to be as short as possible but supplying decent brightness in the speckle image (1 ms). The speckle size was about 4 camera pixels in area to give one speckle per output image pixel after the 2 × 2 bin, smaller than the ideal case but providing higher spatial resolution and the advantage of higher intensities from the binning.

The raw temporal contrast images were calculated with the Matlab functions *mean* and *std*. The contrast difference between the areas containing a vessel and the surrounding areas was calculated and averaged over the area of interest (AOI) to get the relationship between the contrast difference and time. The contrast difference was defined with the
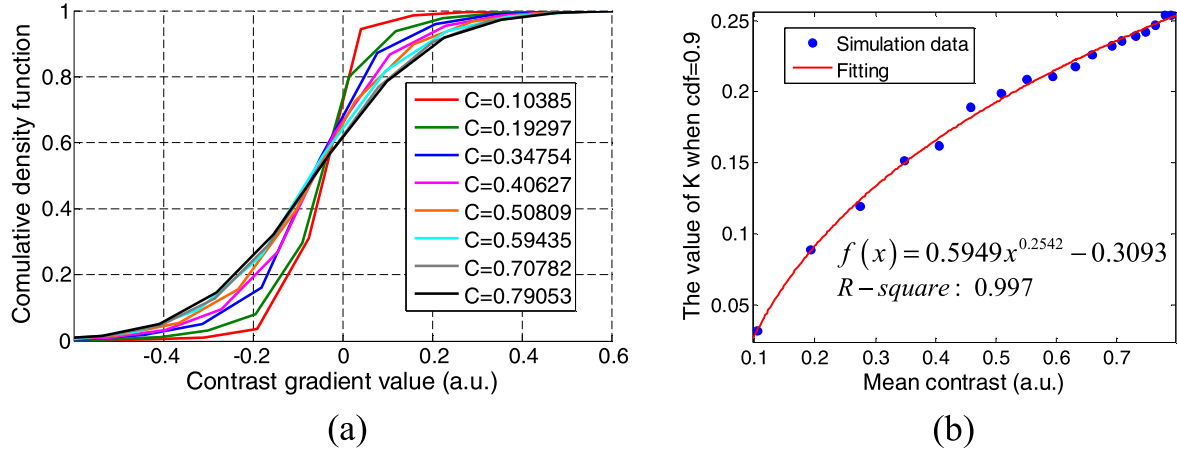
Figure 2. (a) The relationship between the CDF and the contrast values. (b) The relationship between the *K* values and the mean contrast of the speckle image. The *K* value is the value when the CDF is equal to 0.9.

following formula to remove environmental influences:

$$C_d = C_s - C_v \qquad (5)$$

where C_d denotes the contrast difference, C_v represents the mean contrast in the vessel area and C_s denotes the mean contrast in the surrounding area. In the image domain, the raw contrast images were calculated according to the procedure shown in figure 1(a) and KC-ADF with 50 iterations was applied.

5. Results

5.1. Simulation

The first simulation analyzed the relationship between the *K* values and the mean contrast. As described in the methods section, 20 stacks were simulated; therefore 20 curves of the CDF versus the gradient of the contrast were calculated, together with 20 mean contrast values ranging from 0.103 85 to 0.790 53. Eight of the 20 CDF curves are shown in figure 2(a), to show how the CDF changes with the mean contrast. As shown, the value of the contrast gradient, when the CDF was equal to 0.9, increased with the mean contrast. The gradient values when the CDF was equal to 0.9 were extracted, although this was only an approximation due to the resolution limit of the CDF. These extracted *K* values are plotted as a function of the mean contrast in figure 2(b), and ranged from 0.03 to 0.254 when the mean contrast changed from 0.103 85 to 0.790 53. The simulation data were fitted to a polynomial $f(x) = ax^b + c$.

This provides guidance for choosing the *K* value according to the mean contrast. Although the mean contrast in real experiments is an average over both the vessel and the surrounding areas, which is higher than the mean contrast values from vessels alone, we prove in the following paragraphs that *K* values larger than those from the fitting result do not introduce observable influence in the contrast images.

In the second simulation, the contrast image was calculated, as shown in figure 3(b), and the line profile along the middle (900th) row of the raw contrast image is shown in

figure 3(d). Because the central area has lower correlation coefficients, the contrast is lower in this region, although the contrast noise is higher than the contrast difference introduced by the change of correlation coefficients. The mean contrast of figure 3(b) is 0.4357, and therefore *K* was assigned the value of 0.17 according to the fitted equation in figure 2(b). The ADF-processed image with *K* equal to 0.17 using 50 iterations is shown in figure 3(c). Different values for *K* from 0.1 to 0.254 with an increment of 0.01 were tested, and the line profiles of the 900th row of the initial correlation matrix for the processed contrast images with *K* equal to 0.1, 0.17, and 0.254 are shown in figure 3(e). It was found that when the *K* value was 0.1, the line profile had higher noise than that from *K* equal to 0.17, which means noise reduction was not sufficient. More iteration runs can further reduce the noise in this situation but with long processing time and loss of small structures. The results for *K* values of 0.17 and 0.254 are almost identical except that there are more small fluctuations when *K* is equal to 0.254, as can be observed in the magnified image in figure 3(f). This is because a lower *K* value is more proper in these fluctuating areas since the mean contrast values are lower. However, due to the high spatial frequency of these fluctuations, a 3×3 smoothing filter can remove them without significant image blurring, as demonstrated in section 5.2. Another option is to introduce regional adaptive calculation to apply varied *K* values across different regions of the image according to local contrast values.

ADF can therefore preserve the spatial correlation distribution. In addition, to simplify the selection of *K* values, a constant between 0.17 and 0.254, with an optional 3×3 smoothing filter, can be applied to all contrast images.

5.2. The effect of K on the ADF performance in the result of LSCI in vivo

The raw contrast image calculated from three consecutive speckle images of the *in vivo* experiment is shown in figure 4(a). The mean of the contrast image is 0.3078; therefore the *K* value according to figure 2(b) is about 0.13. We applied ADF to the raw contrast image with *K* equal to
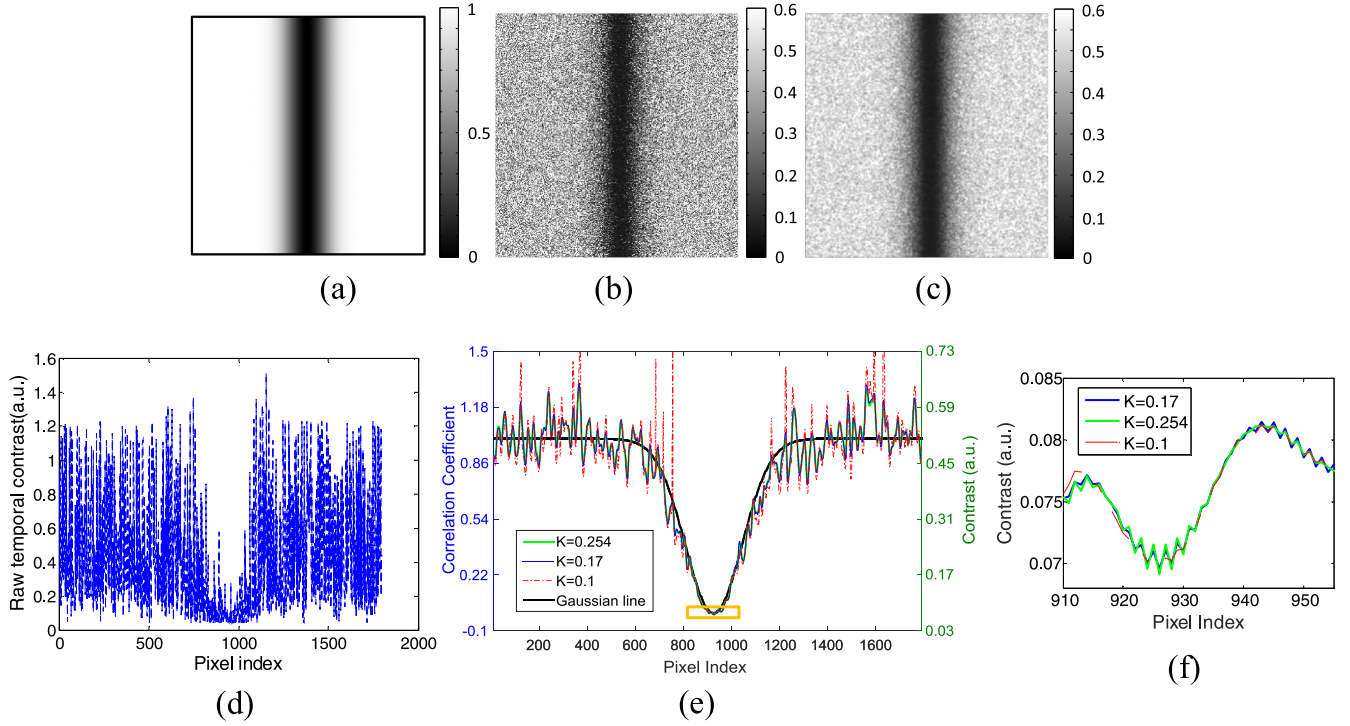
Figure 3. Simulation results: (a) the initial correlation matrix (1800 × 1800 pixels); (b) the raw contrast image; (c) the ADF-processed contrast image with K equal to 0.17; (d) the line profile of the raw contrast along the 900th row; (e) the line profile of the original correlation map and ADF-processed contrast images with K equal to 0.1, 0.17, and 0.254 along the 900th row; and (f) expanded figures of the curves from within the orange square in (e).
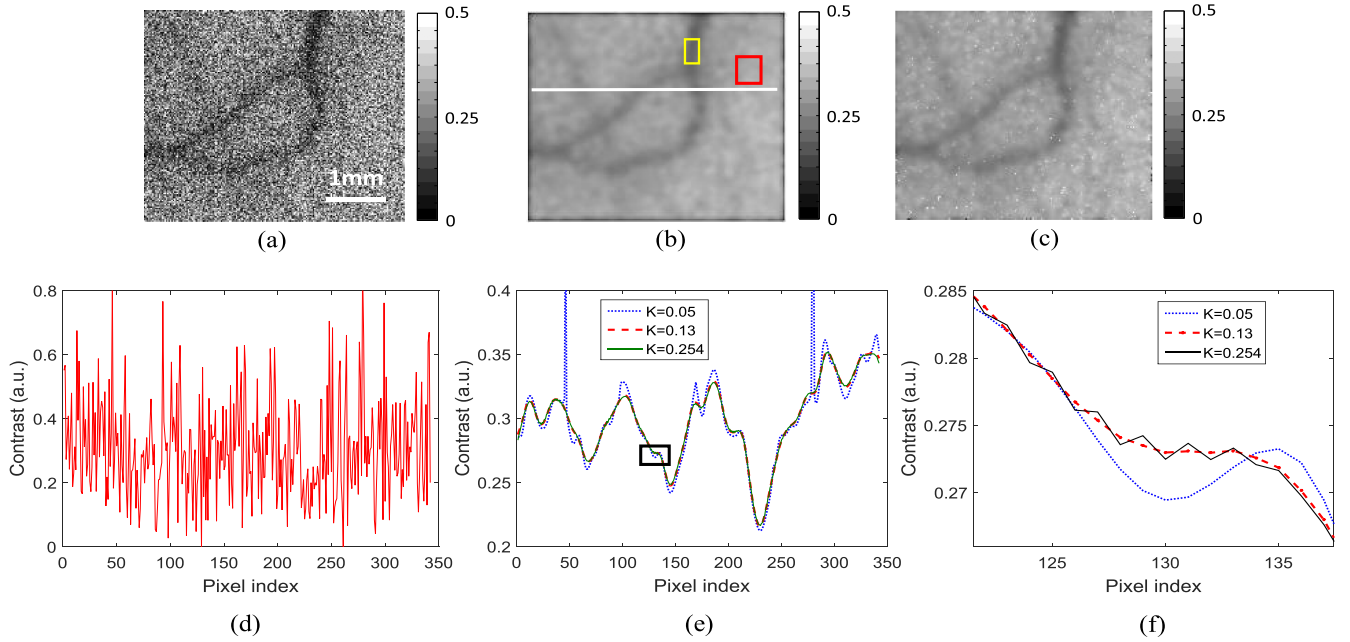

Figure 4. ADF-processed contrast images with different values of K: (a) the raw contrast image; (b) K is equal to 0.13; (c) K is equal to 0.05; (d) the line profile of the raw contrast along the row marked with the white line in (b); (e) the line profile of the same row in (d) with K equal to 0.05, 0.13 and 0.254; and (f) the zoomed-in view of the area marked with a black square in (e).

0.13, 0.254 and 0.05 to compare the effect. The contrast images with K equal to 0.13 and 0.05 are shown in figures 4(b) and (c). Both 0.13 and 0.05 can remove the contrast noise in the image domain but there are white pixels in figure 4(c) indicating that 0.05 is not the best value. The

contrast image with K equal to 0.254 (not presented) is almost identical to the one with K equal to 0.13. Then the line profile along the 125th row of the raw contrast image is shown in figure 4(d), which is overwhelmed by noise. The line profiles of the other processed images are shown in figure 4(e). The
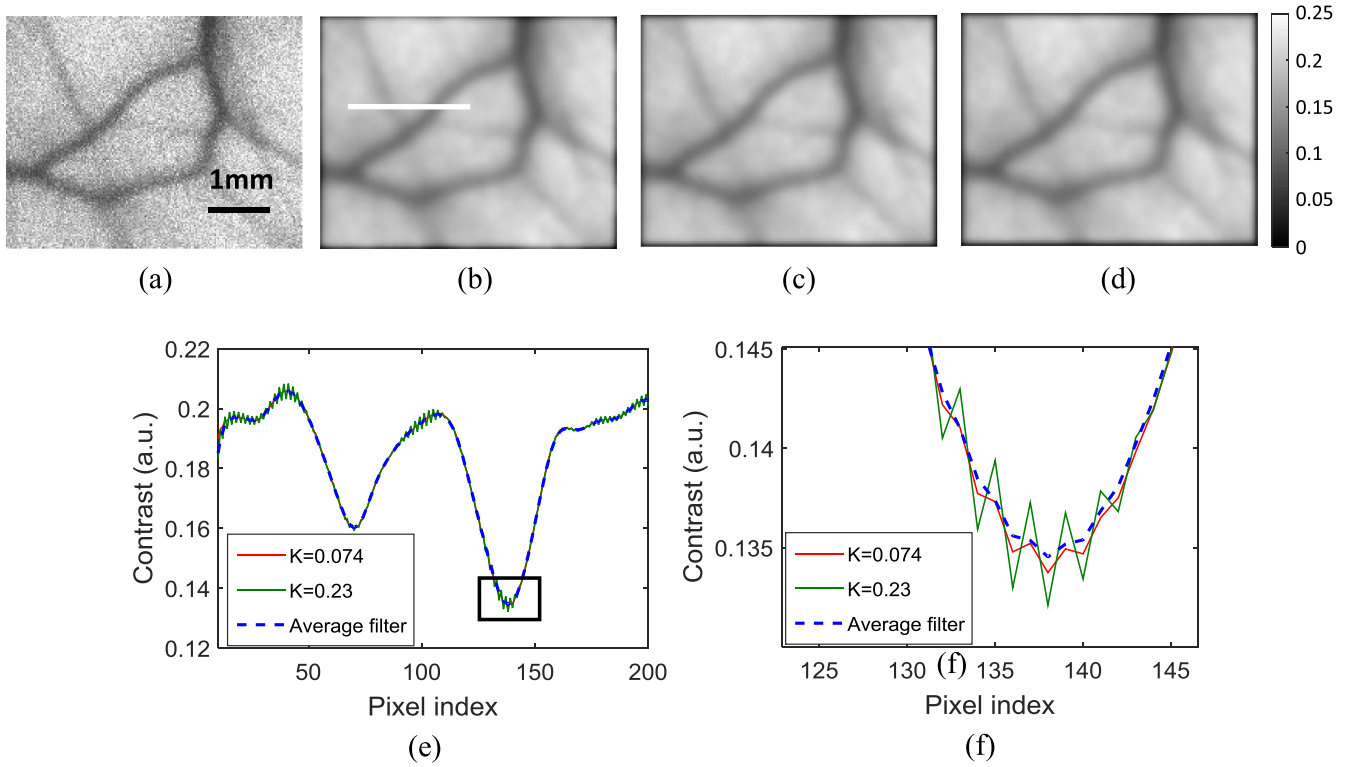
Figure 5. Illustration of high *K* value and average filter performance. (a) The raw contrast image; (b) the KC-ADF-processed contrast image with *K* equal to 0.074; (c) the KC-ADF-processed contrast image with *K* equal to 0.23; (d) the average filter processed image of (c); (e) the line profile of (b)–(d) along the row marked with the white line in (b); and (f) the expanded-scale figures of the area marked with a black square in (e). The image scale is the same as that in figure 4(a).

dashed blue line is the result with *K* equal to 0.05, and the fluctuations correspond to the white pixels in the image domain. The red dashed line and the green line are the result with *K* equal to 0.13 and 0.254 respectively. As in the simulation these two lines are almost identical, except that there are more deviations visible for the green line when viewed with a larger scale in figure 4(f). This also explains why the contrast images with these two *K* values look identical.

The experimental results suggest again that in an image domain the value of *K* can be chosen according to figure 2(b), or simply from a range between the value calculated according to the mean contrast and 0.254. This will not change the appearance of the contrast images. Then in the following experimental data process, we used 0.23 to extract the heartbeat of the mouse.

KC-ADF was further tested using higher-than-optimal *K* values and using an averaging filter to calculate a final contrast image. The temporal contrast was initially calculated from 40 speckle frames acquired with the same experimental setup but with an exposure time equal to 20 ms to produce low contrast values. According to figure 2(b), the mean value of the contrast image decreased to 0.179 corresponding to a *K* value of 0.074. When applying KC-ADF using a larger *K* value of 0.23, more fluctuations were expected; therefore we additionally applied a median filter (3 × 3 pixels) to the contrast image. Figure 5(a) shows the raw contrast image. Figures 5(b)–(d) are the processed contrast images with

K = 0.074, *K* = 0.23 and *K* = 0.23 and additional median filtering. They are nearly identical to the eye, but the line profile for *K* = 0.23 exhibits more fluctuations than the other two lines, as expected. The line profile of *K* = 0.23 plus a median filter shows less fluctuation than that with the 'ideal' *K* value.

5.3. Measurement of rat heartbeat

The contrast difference was calculated according to equation (5) for the AOI in the vessel and surrounding tissue marked with yellow and red rectangles respectively in figure 4(b). Because the contrast in the surrounding area is subtracted from that in the vessel area, higher contrast difference values correspond to higher flow speeds. The contrast difference as a function of time is shown in figure 6(a). It exhibits periodic changes although the shape of the period is not perfect due to noise or the raw speckle images and the low temporal resolution. The power spectrum of the contrast difference and that of the ECG measurement are shown in figure 6(b). The peak frequencies of the LSCI and the ECG in figure 6(b) are close, with values of 6.2 Hz and 6.8 Hz respectively. There are two factors that induced the 0.6 Hz difference. One is the noise in the contrast values as a function of time. Changing the AOI used to calculate the contrast difference can introduce a frequency shift in the range of ±0.2 Hz. This is because of the low SNR in the raw speckle images, which will be elaborated in the discussion section. In addition the cardiac period slightly changes over time.
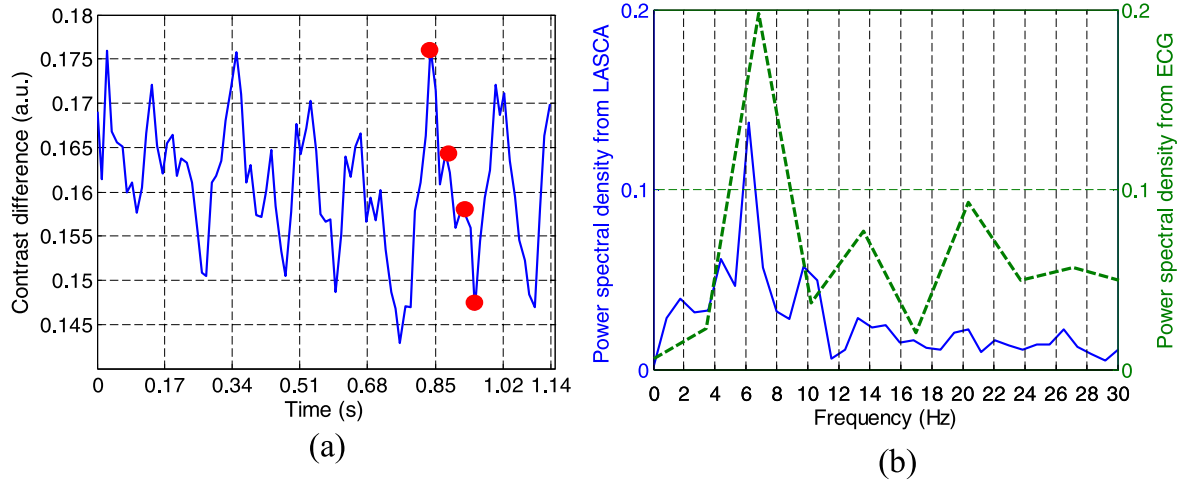
Figure 6. (a) Contrast difference as a function of time, which shows the heartbeat of the rat; (b) the frequency spectrum of (a) and the ECG measurement. The red dots mark four time points demonstrating the contrast changes within a cardiac period.
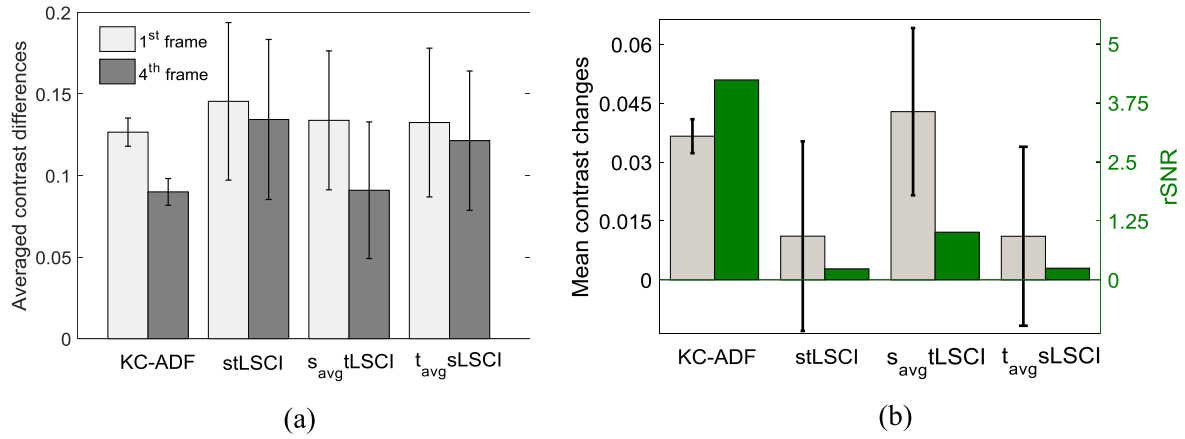

Figure 7. Comparison between different contrast calculation methods: (a) the mean contrast differences calculated using the different methods. The error bars correspond to the standard deviations of the contrast in these areas. (b) The mean contrast change (gray bars) and the rSNR (green bars) for the different methods. The rSNR is the ratio between the mean contrast change and the standard deviation values of the contrast marked with the error bars on the columns.

Table 1. Comparison between the four contrast calculation methods.

	KC-ADF	stLSCI	s_{avg}tLSCI	t_{avg}sLSCI
First frame contrast (Mean ± Std)	0.127 ± 0.0087	0.146 ± 0.048	0.134 ± 0.043	0.133 ± 0.047
Fourth frame (Mean)	0.09	0.1344	0.0905	0.1214
Contrast change	0.0362	0.0115	0.0434	0.0111
rSNR	4.185	0.238	1.019	0.243
Improvement of KC-ADF in rSNR	—	17.584	4.107	17.222
Window ($N_s \times N_s \times N_t$)	$3 \times 3 \times 3$	$3 \times 3 \times 3$	$3 \times 3 \times 3$	$3 \times 3 \times 3$
p-Value for improvement of KC-ADF in rSNR		<0.0001	0.000 15	<0.0001

To demonstrate the improved speed sensitivity and temporal resolution of KC-ADF in an image domain, KC-ADF, stLSCI, s_{avg}tLSCI and t_{avg}sLSCI were applied to the speckle images and the results of four time points marked as red dots in figure 6(a) were chosen to compare these four methods using a kernel size equal to $3 \times 3 \times 3$ ($N_s \times N_s \times N_t$). In KC-ADF, *K* was equal to 0.23 and there were 50 iteration runs. We chose four AOIs from large and small vessels and averaged the contrast difference C_d, the

standard deviation (std) of C_d, and the contrast changes between the first and fourth frames over the four AOIs. The results are shown in figure 7 and the data are listed in table 1. It is clear from figure 7(a) that KC-ADF gives the smallest std, only 18% of those of the other three methods, meaning that KC-ADF has the best noise-suppressing effect. To display the cardiac cycle, the contrast changes need to be larger than the noise, and we define the relative SNR (rSNR) as the contrast change divided by the std to evaluate the ability to
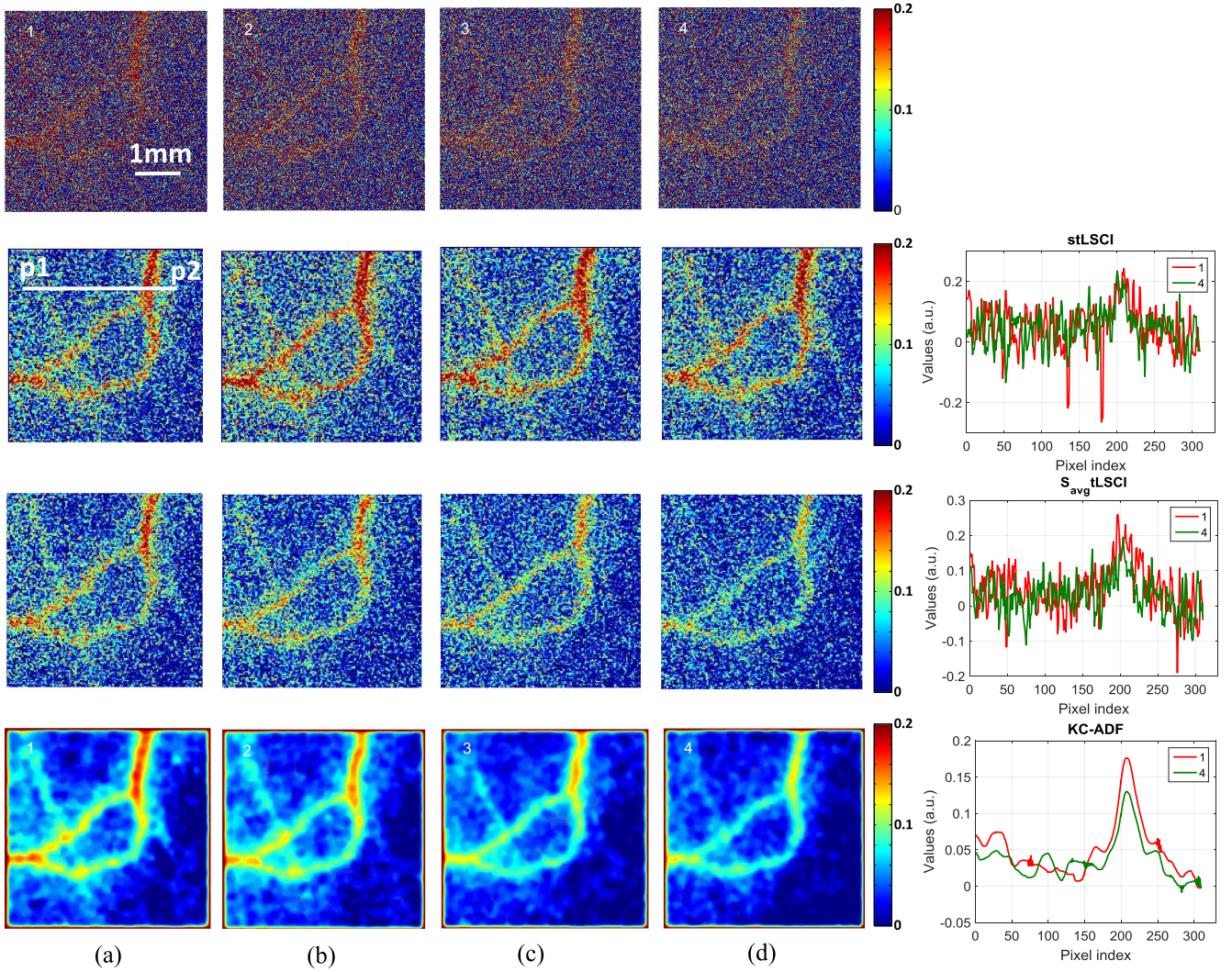
Figure 8. Contrast images (left (a)–(d)) and line profiles (right) over half of a cardiac period. Top row: raw tLSCI contrast difference images; second row: stLSCI contrast difference images and line profiles; third row: s_{avg}tLSCI contrast difference images and line profiles; bottom row: KC-ADF-processed tLSCI contrast difference images and line profiles with *K* equal to 0.23. From (a) to (d): the contrast difference images corresponding to the four time points from left to right shown in figure 6(a).

detect the cardiac cycle. Figure 7(b) shows that although KC-ADF has smaller contrast changes than s_{avg}tLSCI, it produces the highest rSNR thanks to the low std. The rSNR of KC-ADF (4.185) is nearly 18 times that of tLSCI (0.238) and 4 times that of s_{avg}tLSCI (1.019) ($p \leqslant 0.000\,15$; one-sided Student *t*-test). The methods of stLSCI and t_{avg}sLSCI have similar performance in terms of rSNR. Table 1 lists the values of the parameters in figure 7.

The images of the contrast difference at the four time points are shown in figure 8 to further demonstrate the improved speed sensitivity and the temporal resolution in the image domain. Again, higher contrast difference values correspond to higher flow speed. Pseudo-colors were added corresponding to the contrast difference values. The top row shows the contrast difference images of the raw tLSCI. Due to the low SNR, the contrast changes over time are barely detected. The second row shows the contrast difference from stLSCI. Although the SNR increases compared to that of the tLSCI, the speed changes are still unperceivable due to the

low rSNR. The third row shows the contrast difference image with s_{avg}tLSCI. The cardiac cycle can be identified from the decreased area of red color. This can be explained by the increased rSNR, which is four times that of stLSCI according to table 1. But since red color exists in all the four frames, s_{avg}tLSCI cannot totally distinguish the speed changes. Compared with the fourth row, the noise with s_{avg}tLSCI is still high. In the fourth row, the results with KC-ADF exhibit totally different colors changing from red to yellow in the vessel area during half a cardiac period and therefore clearly show the flow speed changes introduced by the heartbeat.

The line profiles along line p1–p2 of the contrast in frame 1 and frame 4 for the three processing methods are provided on the right side of figure 8. Clearly the contrast change between the two frames is obscured by noise for tLSCI. It is possible to detect a slightly larger contrast difference for the large vessel for frame 1 compared with frame 4 with s_{avg}tLSCI. The line profiles for KC-ADF are clearly
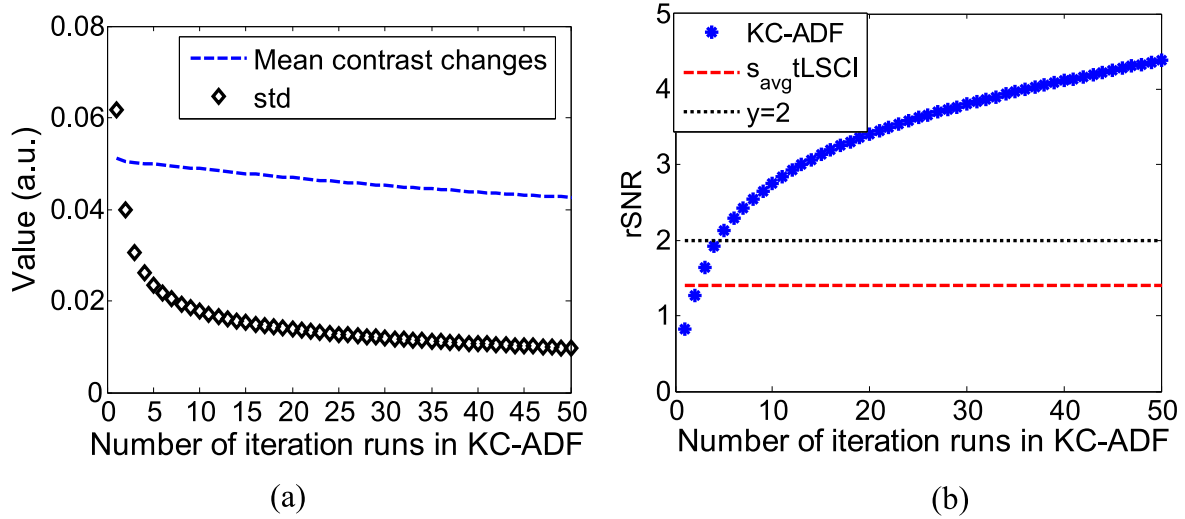
Figure 9. The performance of KC-ADF with different numbers of iterations. (a) The mean contrast difference changes and the std as a function of the iteration runs; (b) the rSNR as a function of the iteration runs.

distinguished for the vessels, which is consistent with the observable color changes in the contrast images.

The contrast difference was calculated from three successive speckle frames, that is, the minimum number for contrast calculation, and the KC-ADF-processed contrast images display contrast changes that cannot be identified with the other methods; therefore, the temporal resolution and the speed sensitivity are improved.

5.4. Number of iterations

It is known that the number of iterations of ADF impacts performance. Therefore we investigated the std and the contrast changes as a function of iteration runs from 1 to 50 with a *K* value of 0.23. The results are shown in figure 9(a). The changes of mean contrast between the first frame and the fourth frame slightly decrease with the increase of the iteration runs, but the std of the contrast difference decreases sharply when the iteration runs increase from 1 to about 7 and then decreases slowly. Theoretically the mean contrast changes from the speed difference can be easily identified in the image domain when the rSNR is higher than 2, i.e. the mean contrast change is over the high or the low limit of the std. From figure 9(b), the rSNR of KC-ADF increases to higher than 2 when the number of iterations is 5. The rSNR of KC-ADF is higher than that of s_{avg}tLSCI only after running two iterations according to figure 9(b). Running more iterations can maximally remove statistical residual noise. This does not introduce a significant border blur because ADF smooths the image perpendicular to the vessels. The processing time of KC-ADF in our experiment, using a 3.4 GHz Intel i7 desktop computer for an image size of 322 × 361 pixels, increased from approximately 0.07 to 0.24 s when the number of iterations was increased from 2 to 50. When the *K* value was calculated from the mean contrast instead of retaining the fixed value of 0.23, the processing time was still in the same range.

6. Discussion and conclusion

The noise level can be suppressed by using a low-noise camera but statistical residual noise is inevitable. In addition, decreasing the number of speckle images for calculating one frame of a temporal contrast image is still desirable to achieve higher temporal resolution. This will unavoidably induce higher statistical residuals, i.e. contrast noise. Therefore our method is also applicable to this situation. In this paper we demonstrate better speed sensitivity and temporal resolution than current spatial averaging and temporal–spatial averaging imaging techniques when the speckle images are acquired with the same experimental setup.

The CMOS camera used in the experiment was industrial grade. The dark current increased during the data acquisition because the camera's temperature increased. In addition, to achieve a high frame rate the pixels were binned, increasing the dark current noise. The 1 ms exposure time and the laser power restriction for the animal experiment limited the signal intensity. In the end, the background intensity was as high as 50 (gray-level digital number) when the signals were around 100. Therefore the contrast images show very low SNRs, especially when only three speckle frames were included in the calculation. This also explains why in figure 6 the three phases corresponding to the cardiac diastole, atrial systole and ventricular systole stages are not visible for all periods in figure 6(a). But the frequency of the heartbeat was clearly caught and KC-ADF greatly improved the quality of contrast images even when the SNR of the raw speckle images was low.

In figure 4, the proper *K* value of 0.13 was calculated based on the mean of the contrast image according to the relationship shown in figure 2(b). Since the simulation and the experiment *in vivo* may not be the same, we calculated the CDF of the gradient of figure 4(a) and located the *K* value when the CDF was equal to 0.9. Thus, the *K* value is 0.148, slightly higher than 0.13, but this divergence does not introduce a perceivable difference in the processed images. This further suggests the applicability of the relationship in figure 2(b).
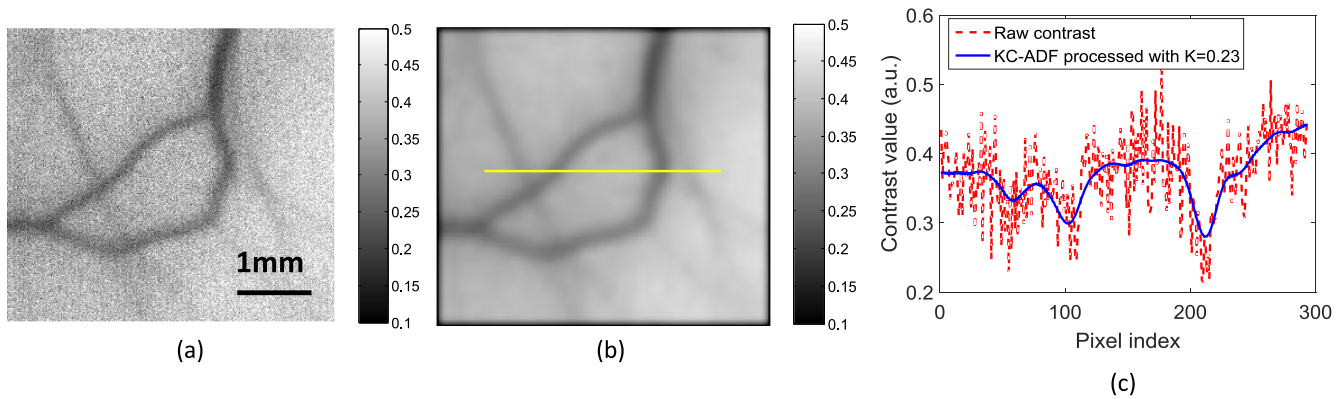
Figure 10. Demonstration of the noise reduction of KC-ADF in contrast images calculated from 200 speckle frames. (a) The raw contrast image calculated from 200 speckle frames; (b) the KC-ADF-processed contrast image in (a) with *K* equal to 0.23; (c) the contrast profile along the yellow line in (b), showing clear noise suppression.
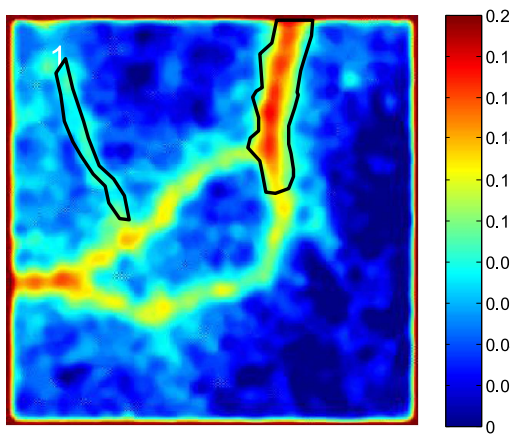

Figure 11. Areas for the comparison of the improvement of KC-ADF enhancement for large and small vessels.

In the above sections, we showed the effect of KC-ADF on contrast images calculated from three speckle frames. Here we demonstrate the noise reduction effect of KC-ADF on a contrast image calculated from 200 speckle frames, as shown in figure 10. The noise of the raw contrast image from 200 frames in figure 10(a) is lower than that of the contrast image from three speckle frames shown in figure 4(a). However the KC-ADF-processed contrast image in figure 10(b) still shows an obvious noise suppression effect, which can be seen in the line profile presented in figure 10(c).

To investigate whether the noise suppression effect was different for large and small vessels, we took the raw and KC-ADF-processed contrast images in figures 8(a) and (d) and manually chose areas covering parts of the larger and smaller vessels. The areas for comparison are shown in figure 11 with the test parameters listed in table 2. SNR improvement (the SNR of the KC-ADF-processed image divided by the SNR of the raw image) is much greater for the small vessel (about 16 times) than for the large vessel (9–10 times). This is because the noise level in the small-vessel area in the raw images is higher and accordingly KC-ADF produces the best improvement. The rSNR improvement (the rSNR of the KC-ADF-processed image divided by the rSNR of the raw image) of the small vessel is also greater than that

of the large vessel with values of 19.11 and 11.82 respectively.

As mentioned in the introduction, Rege has provided an anisotropic processing method (aLSCI) for speckle images. Compared to KC-ADF, this method provides better vessel border sharpness, but it has the disadvantages of increased time and calculation complexity, depending on a pre-tLSCI calculation from at least 75 speckle images for a good result. In addition, the improvement of aLSCI in SNR is smaller than that of KC-ADF. Another SNR improvement method, the random estimator method proposed by P. Miao [7], also provides good vessel border sharpness, but the improvement in SNR is several times smaller than that of KC-ADF.

KC-ADF is based on the spatial averaging of noise, so it does not change the statistical expectation of the contrast. Therefore KC-ADF has the same measurement range as tLSCI for the same experimental setup if the analysis is based on contrast expectations. But the visible range and temporal resolution are improved with KC-ADF because of the improved rSNR. The rSNR of KC-ADF is nearly 18 times that of tLSCI and 4 times that of s_{avg}tLSCI. The spatial resolution in this paper means the smallest vessel size that can be distinguished in the speckle contrast images. It is affected by both the spatial resolution limit from the imaging system and the noise level of the contrast images. Because KC-ADF spatially averages the noise, the spatial resolution limit from the imaging system is the same as that of the raw speckle contrast images. But because noise is reduced, smaller vessels can be distinguished—for example, more vessels are displayed in figures 5(b)–(c) than in figure 5(a). However it can also be noted that the improvement of the SNR of KC-ADF comes at the cost of image sharpness due to the averaging effect and fewer iteration runs can better preserve sharpness.

KC-ADF is an image processing method, so the quality of the processed image is limited by the quality of the raw speckle and raw contrast images. A higher image acquisition frame rate and shorter exposure time are necessary for capturing fast changes in flow speed, but this may decrease the SNR of the speckle images due to the lower signal intensity and consequently decrease the SNR of the contrast images. A stable experimental environment is important especially when

Table 2. Comparison between large vessel and small vessel.

		Figure 8(a)		Figure 8(d)	
		Large vessel	Small vessel	Large vessel	Small vessel
Raw	mean $\pm$ std	0.16 $\pm$ 0.11	0.07 $\pm$ 0.15	0.12 $\pm$ 0.11	0.05 $\pm$ 0.14
	SNR (mean/std)	1.45	0.51	1.12	0.35
	rSNR	0.30	0.17		
KC-ADF	mean $\pm$ std	0.15 $\pm$ 0.01	0.08 $\pm$ 0.01	0.11 $\pm$ 0.01	0.05 $\pm$ 0.01
	SNR (mean/std)	13.18	8.40	11.32	5.55
	rSNR	3.54	3.21		
SNR improvement	9.12	16.58	10.08	15.91	
rSNR improvement	11.82	19.11			

the contrast is calculated from time-sequential speckle images.

In conclusion, in this paper we demonstrate that KC-ADF can suppress contrast noise. In contrast to other methods for determining the parameter K for ADF, KC-ADF can select the K value only based on the mean contrast and a value between 0.17 and 0.254 was found to effectively suppress contrast noise. A median filter of 3×3 pixels is an option to remove the fluctuations introduced by high K values although this is not necessary for imaging. Combining KC-ADF and contrast calculation with three sequential speckle images, speed sensitivity and temporal resolution are improved because of an enhanced SNR compared with those of stLSCI, s_{avg}tLSCI and t_{avg}sLSCI. The rat heartbeat as high as 390 bpm was captured and illustrated in the image domain based on low-SNR speckle images recorded by an industrial camera.

Acknowledgments

ORCID iDs

Ru Zhang ⬤ https://orcid.org/0000-0003-3795-4556

References

[1] Duncan D D, Kirkpatrick S J and Wang R K 2008 *J. Opt. Soc. Am.* A **25** 9–15

[2] Dunn A K, Bolay H, Moskowitz M A and Boas D A 2001 *J. Cerebral Blood Flow Metabolism* **21** 195–201

[3] Le T M, Paul J S, Al-Nashash H, Tan A, Luft A, Sheu F and Ong S 2007 *IEEE Trans. Med. Imaging* **26** 833–42

[4] Duncan D D and Kirkpatrick S J 2008 *SPIE-BiOS Photonics West* pp 685802–6

[5] Miao P, Li M H, Fontenelle H, Bezerianos A, Qiu Y H and Tong S B 2009 *IEEE Trans. Biomed. Eng. Imaging* **56** 1127–33

[6] Miao P, Li N, Thakor N V and Tong S 2010 *Opt. Express* **18** 218–36

[7] Qiu J, Li Y, Huang Q, Wang Y and Li P 2013 *Opt. Express* **21** 28902–13

[8] Thompson O, Andrews M and Hirst E 2011 *Biomed. Opt. Express* **2** 1021–9

[9] Zeng Y, Wang M, Feng G, Liang X and Yang G 2013 *Opt. Lett.* **38** 1313–5

[10] Rege A, Senarathna J, Li N and Thakor N V 2012 *IEEE Trans. Biomed. Eng.* **59** 1272–80

[11] Murari K, Li N, Rege A, Jia X, All A and Thakor N 2007 *Appl. Opt.* **46** 5340–6

[12] Aylward S R and Bullitt E 2002 *IEEE Trans. Med. Imaging* **21** 61–75

[13] Yu Y and Acton S T 2002 *IEEE Trans. Image Processing* **11** 1260–70

[14] Abd-Elmoniem K Z, Youssef A and Kadah Y M 2002 *IEEE Trans. Biomed. Eng.* **49** 997–1014

[15] Bini A A and Bhat M S 2014 *Multidimens. Syst. Signal Process.* **25** 41–65

[16] Perona P and Malik J 1990 *IEEE Trans. Pattern Anal. Mach. Intell.* **12** 629–39

[17] Black M J, Sapiro G, Marimont D H and Heeger D 1998 *IEEE Trans. Image Process.* **7** 421–32

[18] Yang Z and Fox M D 2004 *EURASIP J. Appl. Signal Process.* **2004** 2492–502

[19] Ovireddy S and Muthusamy E 2014 *Ultrason. Imaging* **36** 112–32

[20] Canny J 1986 *IEEE Trans. Pattern Anal. Mach. Intell.* **8** 679–98

[21] Song L, Zhou Z, Wang X, Zhao X and Elson D S 2016 *Biomed. Opt. Express* **7** 798–809

[22] Kirkpatrick S J, Duncan D D and Wells-Gray E M 2008 *Opt. Lett.* **33** 2886–8